Chemical Engineering Journal 428 (2022) 131165

Contents lists available at ScienceDirect

Chemical Engineering Journal

journal homepage: www.elsevier.com/locate/cej

# Lanthanide dopant stabilized $Ti^{3+}$ state and supersensitive $Ti^{3+}$ -based multiparametric luminescent thermometer in $SrTiO_3$:$Ln^{3+}$ ($Ln^{3+}$ = $Lu^{3+}$, $La^{3+}$, $Tb^{3+}$) nanocrystals

W. Piotrowski [a], M. Kuchowicz [b], M. Dramićanin [c], L. Marciniak [a,*]

[a] Institute of Low Temperature and Structure Research, Polish Academy of Sciences, Okólna 2, 50-422 Wroclaw, Poland
[b] Institute of Experimental Physics, Faculty of Physics and Astronomy, University of Wroclaw, Wroclaw 50-204, Poland
[c] Vinča Institute of Nuclear Sciences - National Institute of the Republic of Serbia, University of Belgrade, P.O. Box 522, Belgrade 11001, Serbia

ARTICLE INFO

*Keywords:*
Luminescent thermometry
$SrTiO_3$ nanoparticles
Titanium $Ti^{3+}$ emission
Cryogenic temperature measurements
Emission decays

ABSTRACT

Herein, we show that the substitution of $Sr^{2+}$ by trivalent lanthanide ions ($Lu^{3+}$, $La^{3+}$, $Tb^{3+}$) in $SrTiO_3$ nanocrystals stabilizes and enhances $Ti^{3+}$ near-infrared emission (around 800 nm). This emission occurs from the 6-fold coordinated $Ti^{3+}$ luminescent centers that appear in the vacancy–$Ti^{3+}$–O form after lanthanide doping into the $Sr^{2+}$ site. The strong dependence of the $Ti^{3+}$ emission on temperature provided means for the tailored chemical engineering of luminescent nanonthermometers able to read the temperature in three ways: from the changes in $Ti^{3+}$ emission intensity, excited-state lifetime, and from the ratio of $Tb^{3+}$ and $Ti^{3+}$ emission intensities. We demonstrated the unprecedented temperature sensitivity of the lifetime-based luminescent thermometer (8.83% $K^{-1}$) with $SrTiO_3$:$Tb^{3+}$, along with exceptional repeatability in measurements.

## 1. Introduction

Continuously growing scientific attention on the utilization of inorganic phosphors doped with transition metal ions (TM) for remote temperature sensing observed in recent years results from their several highly important advantages with respect to the other types of dopants used for this purpose[1-12]. First of them is the high susceptibility of TM luminescence to temperature changes which enables the development of highly sensitive temperature probes[13-15]. Moreover, the significantly higher absorption cross-section of the *d-d* type electronic transitions occurred in TM with respect to for instance *f-f* transitions of lanthanide ions ($Ln^{3+}$) enables obtaining bright luminescence which facilitates signal collection[16-19]. Additionally, the strong susceptibility of spectroscopic properties of the TM doped phosphors, like the spectral range of optical response and the luminescence thermal quenching rate, on the local ions environment enables facile modulation of the thermometric performance of such luminescent-based temperature probe almost on demand[8,13,15,20]. The optimal spectral range in which a given luminescent thermometer should work strongly depends on the type of its application. Luminescent thermometers emitting in the visible range are definitely cheaper to use, because the cost of the equipment required to register their luminescence is much lower than those emitting in the infrared range. However, for biomedical applications, for example, this spectral range is not particularly useful due to the high scattering and absorption of biological media in the visible range. Therefore, in this case, it is much more advantageous to develop infrared-emitting luminescent thermometers. Although the studies devoted to the temperature dependence of the TM emission intensity are significantly important to understand the mechanism of the thermal quenching of the emission, the reliability of the temperature readout based on the luminescent thermometry (LT) which exploits single band emission as a thermometric parameter is questionable[21-26]. For this reason, a ratiometric LT that exploits the luminescence intensity ratio of either a different emission bands of TM or involves an emission band of the lanthanide ion co-dopant as an internal luminescent reference has been proposed[1]. However, as shown recently, the introduction of the lanthanide ion itself may strongly modify the local ions environment and thus the luminescence thermal quenching rate[27].

In this study, we show that even more far-reaching consequences may result from the introduction of the lanthanide ions into $SrTiO_3$ structure. The difference in the electric charges and ionic radii between $Ln^{3+}$ dopants and $Sr^{2+}$ in the $SrTiO_3$ host material may lead to the stabilization of the $Ti^{3+}$ oxidation state and appearance of the $Ti^{3+}$ emission. Upon suitable $Ln^{3+}$ doping, the intensity enhancement of $Ti^{3+}$

* Corresponding author.
*E-mail address:* l.marciniak@intibs.pl (L. Marciniak).

https://doi.org/10.1016/j.cej.2021.131165
Received 30 May 2021; Received in revised form 21 June 2021; Accepted 1 July 2021
Available online 8 July 2021

emission and the spectacular elongation of the lifetime of the $^2E$ excited state can be obtained. Taking advantage of the strong thermal dependence of the spectroscopic properties of the $Ti^{3+}$ ions in this host material, the luminescent thermometer exploiting different thermometric approaches has been proposed and carefully evaluated, i.e. $Ti^{3+}$ emission intensity-based LT, $Ti^{3+}$ lifetime based LT, and the ratiometric approach which involves $Ti^{3+}$ to $Tb^{3+}$ emission intensity ratio. Since the $Ti^{3+}$ based luminescent thermometry has been scarcely explored so far, the presented studies are an important contribution to understanding the spectroscopic properties of the $Ti^{3+}$ ions and to the development of the highly sensitive luminescent thermometry. Further, to the best of our knowledge, this study presents the highest ever reported relative sensitivity of the lifetime based LT of $S_R = 8.83\%\ K^{-1}$ obtained using $SrTiO_3:Tb^{3+}$ nanocrystals. This undoubtedly indicates the high applicative potential of these nanocrystals for the remote temperature sensing.

## 2. Experimental

The $SrTiO_3$, $SrTiO_3$:x% $Ln^{3+}$ (x = 0.1, 0.2, 0.5, 1, 2, 5; $Ln^{3+} = La^{3+}$, $Lu^{3+}$) and $SrTiO_3$:1% $Tb^{3+}$ nanopowders were synthesized using the modified Pechini method[28]. Lanthanum oxide ($La_2O_3$ of 99.99% purity from Stanford Materials Corporation), lutetium oxide ($Lu_2O_3$ with 99.995% purity from Stanford Materials Corporation), terbium oxide ($Tb_4O_7$ with 99.999% purity from Stanford Materials Corporation) strontium nitrate ($Sr(NO_3)_2$ of 99.9965% purity from Alfa Aesar), titanium(IV) n-butoxide ($Ti(OC_4H_9)_4$ with 99+% purity from Alfa Aesar), 2,4-Pentanedione ($C_5H_8O_2$ with 99% purity from Alfa Aesar) and citric acid ($C_6H_8O_7$ of 99% purity from Sigma Aldrich) were used as the starting compounds. An appropriate amount of nitrates was dissolved in deionized water. In the case of the $Ln^{3+}$ co-doped nanocrystals, to obtain nitrates from oxides, their stoichiometric amounts were diluted in a water solution of ultrapure nitric acid. Then, all aqueous solutions of nitrates were mixed and, subsequently, the appropriate amount of Ti $(OC_4H_9)_4$ was measured out into a small laboratory beaker, then a solution of 2,4-pentanedione in the stoichiometric amount was added to stabilize $Ti(OC_4H_9)_4$ solution. The contents of the beaker were gently stirred to obtain a transparent, yellowish solution, which then was combined with the nitrate solution. After this, the solution was mixed with anhydrous citric acid. Subsequently, the obtained solution was dried for 1 week at 363 K until a resin was formed and annealed at 1173 K for 3 h in air atmosphere.

All of the synthesized materials were examined by X-ray powder diffraction (XRPD) measurements carried out on PANalitycal X'Pert diffractometer, equipped with an Anton Paar TCU 1000 N temperature control unit, using Ni-filtered Cu-$K_\alpha$ radiation (V = 40 kV, I = 30 mA).

Transmission electron microscope (TEM) and selected-area electron diffraction (SAED) images were taken using Philips CM-20 SuperTwin TEM microscope. The samples were dispersed in methanol, and a droplet of such suspension was put on a microscope copper grid. Next, the samples were dried and purified in a plasma cleaner. Studies were performed in a conventional TEM procedure with 160 kV parallel beam electron energy. The sizes were determined manually using ImageJ software by measuring the longest linear size (Feret diameter) of each particle.

The emission spectra were measured using the 400 nm excitation lines from a laser diode and a Silver-Nova Super Range TEC spectrometer from Stellarnet (1 nm spectral resolution) as a detector. The temperature of the sample was controlled using a THMS 600 heating–cooling stage from Linkam (0.1 K temperature stability and 0.1 K set point resolution).

The X-ray Photoelectron Spectroscopy (XPS) has been used for surface chemical composition analysis. The non-monochromatized X-ray Mg Kα excitation source was used. All measurements have been performed using an AES/XPS system EA10 (Leybold-Heraeus GmbH, Cologne, Germany). The overall resolution of the spectrometer during the measurements was 0.96 eV as a full width of half maximum (FWHM) of the Ag3d5/2 line. During measurements pressure was kept at a 10–9 mbar range. All acquired spectra were calibrated to adventitious carbon C1s at 285 eV. After subtraction of the Shirley-type background, the core-level spectra were decomposed into main components with mixed Gaussian–Lorentzian lines (70% G + 30% L for majority of photo-peaks) by a non-linear least squares curve-fitting procedure, using CasaXPS software. The atomic concentration was determined on the basis of XPS spectra analysis, taking into account the presence of individual elements O, C, Sr and Ti.

The excitation spectra and luminescence decay profiles were recorded using a FLS1000 Fluorescence spectrometer from Edinburgh Instruments (0.1 nm spectral resolution) equipped with a halogen lamp and μFlash lamp as an excitation sources and Hamamatsu R928P side window photomultiplier tube as a detector. The emission and excitation spectra at 10 K were measured using helium cryostat.

The average lifetimes of the excited states were calculated from the experimental data fit to the double exponential function using (Eq. S1 and S2). Emission spectra and the luminescence decay profiles were measured every 10 K.

## 3. Results and discussion

### 3.1. Structural and morphological characterization

$SrTiO_3$ crystallizes in the cubic system of centrosymmetric Pm-3 m space group with lattice constant a = 3.90528 Å. It belongs to the family of perovskite compounds of the $ABX_3$ general chemical formula, where 'A' is a larger cation than 'B' and the X is an anion (in most cases - oxygen $O^{2-}$). In strontium titanate, the 'B' site is occupied by $Ti^{4+}$ ions in 6-fold octahedral sites with $O_h$ symmetry (Fig. 1a), while in the 'A' site, $Sr^{2+}$ ions are located in the vacancy spaces between the 'A' octahedrons in pseudo-12-fold cuboctahedral coordination. The comparison of the ionic radii reveals that the $Sr^{2+}$ site (Shannon ionic radius equals 144 pm for $Sr^{2+}$ in 12-fold coordination) is more suitable for $Ln^{3+}$ substitution than $Ti^{4+}$ (60.5 pm for 6-fold $Ti^{4+}$). Since, the ionic radii have not been calculated for 12-fold coordination of most of $Ln^{3+}$ ions (expect $La^{3+}$ - equals 136 pm), the effective ionic radii of $Ln^{3+}$ ions in its preferential coordination will be used in the discussion of this work (10-fold $La^{3+}$: 127 pm and 8-fold $Lu^{3+}$: 97.7 pm). On the other hand, the charge difference between $Sr^{2+}$ and $Ln^{3+}$ has been noted. That may be concluded that the incorporation of $Ln^{3+}$ ions is $SrTiO_3$ matrix generate the defects in a structure that may be compensated by 3 routes: strontium vacancies, titanium vacancies or conduction electrons and expressed by the following formulas: $Sr_{1-3/2x}Ln_xTiO_3$, $SrTi_{1-x}Ln_xO_{3-\delta}$ or $Sr_{1-x/2}Ti_{1-x/2}Ln_xO_3$, respectively [29-32]. However, so far in some reports, the perovskite-type titanate structures $LnTiO_3$ with most of $Ln^{3+}$ ions have been successfully presented with appropriate charge distribution of the form $Ln^{3+}Ti^{3+}O_3$ in comparison to $Sr^{2+}Ti^{4+}O_3$. As it will be shown in this manuscript, it is confirmed that that the incorporation of $Ln^{3+}$ ions in $SrTiO_3$ leads to the creation of oxygen vacancies ([ ]–$Ti^{3+}$–O, where [ ] - oxygen vacancy) and thus local defected 6-fold coordinated $Ti^{3+}$ centers adjacent to $Ln^{3+}$ polyhedrons [33]. The comparison of the obtained XRPD patterns of synthesized $SrTiO_3$ nanocrystals undoped and doped with $La^{3+}$, $Lu^{3+}$ and $Tb^{3+}$ ions with the reference data (ICSD 5229) confirms the phase purity of obtained phosphors (Fig. 1b, Figure S1-S2, see also Figure S3 and S4 for Rietveld refinement analysis). No additional reflections can be observed in XRPD after $Ln^{3+}$ doping which is in agreement with the previously published reports [34,35]. The careful XRPD analysis indicates that the introduction of $La^{3+}$ causes the shift of the XRPD reflections toward higher angles which is associated with the reduction of the unit cell size. This effect is expected since the ionic radii of $Sr^{2+}$ is larger with respect to the $La^{3+}$ ones. However, for $La^{3+}$ doping concentrations>0.2% a gradual shift of the XRPD reflections toward smaller angles was observed. This effect may be explained in terms of either (i) substitution of the $Ti^{4+}$ ions by the $La^{3+}$

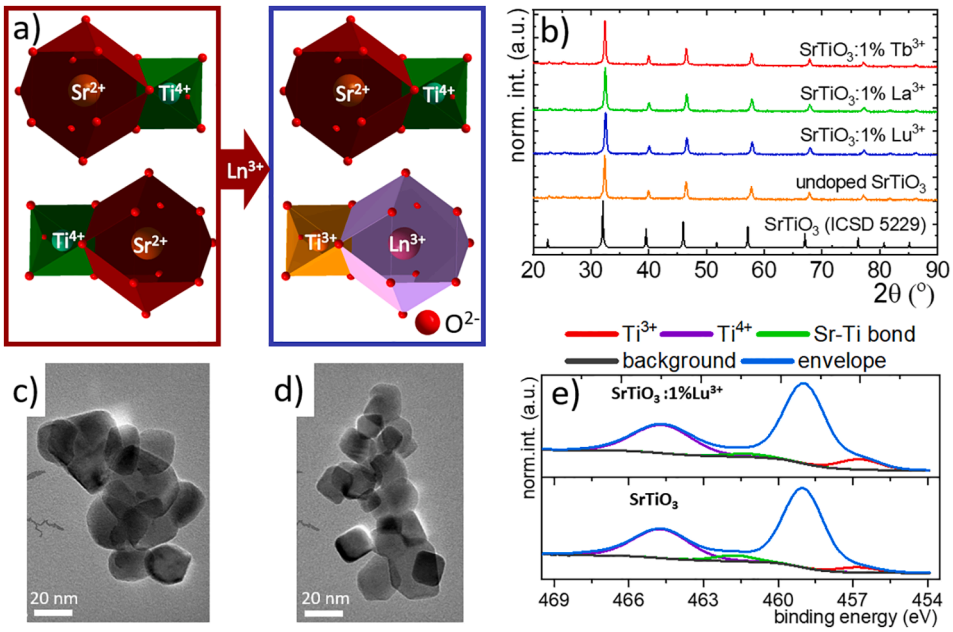


**Fig. 1.** Structural characterization of synthesized materials: the polyhedral visualization of substitution of pseudo-12-fold $Sr^{2+}$ sites with $Ln^{3+}$ ions in the $SrTiO_3$ structure – a; the X-ray diffraction patterns of $SrTiO_3$ with different $Ln^{3+}$ dopants – b; the representative TEM images (scale bar: 20 nm) of undoped $SrTiO_3$ – c and doped with 2% $Lu^{3+}$ – d; XPS – e.

ions or (ii) by the gradual reduction of the $Ti^{4+}$ to $Ti^{3+}$ (ionic radii of $Ti^{3+}$ is 67 pm) associated with the introduction of the $La^{3+}$ ions according to the mechanism described above. Since the ionic radii of $La^{3+}$ is twice larger than the $Ti^{4+}$ counterpart the second hypothesis is only possible. The shift of the XRPD peak positions of $SrTiO_3$:$Ln^{3+}$ patterns by 0.06–0.15° toward higher angles in respect to the undoped $SrTiO_3$ sample corresponds with the contraction of the cell size related to the introduction of $Ln^{3+}$ ions with the lower ionic radii to the $Sr^{2+}$ sites. The transition electron microscopy (TEM) images of representative $SrTiO_3$ and $SrTiO_3$:2% $Lu^{3+}$ materials indicate that they consist of well-crystallized and mostly agglomerated particles of average size around 30 ± 8 nm (Fig. 1c, d, additional TEM images can be found in Figure S5 and Figure S6). Further, the selected-area electron diffraction (SAED) image produced for a single crystal of undoped $SrTiO_3$ powder assures the entire crystallization in the cubic system by the lack of the reflection rings and well-ordered location of the reflection spots corresponding with the cubic system (Figure S7, histogram of particle size distributions are shown in Figure S8). The XPS measurements confirms the presence of the some signal associated with $Ti^{3+}$ in the case of the un-doped $SrTiO_3$ (Fig. 1e, Figure S9). However, the increase of the $Lu^{3+}$ ions concentration to 1% leads to the meaningful increase of the number of $Ti^{3+}$ ions.

### 3.2. Luminescent properties characterization

The $SrTiO_3$ host material can be considered as optically inactive due to the $d^0$ electronic configuration of $Ti^{4+}$ ions. Hence the absorption or emission bands result from the $O^{2-}\rightarrow Ti^{4+}$ or $Ti^{4+}\rightarrow O^{2-}$ charge transfer transitions, respectively. However, the emission intensity of $Ti^{4+}\rightarrow O^{2-}$ is expected to be of rather low intensity. The previously described reduction of the $Ti^{4+}$ to the $Ti^{3+}$ by the introduction of the $Ln^{3+}$ ions causes significant changes in the luminescent properties of the $SrTiO_3$:$Ln^{3+}$. The spectroscopic properties of the $Ti^{3+}$ ions located in the octahedral sites with $O_h$ symmetry may be described with the configurational coordinate diagram (Fig. 2a). For the $3d^1$ electron configuration there are no crystal field induced splittings of energy levels, so the energy levels scheme is a simple two-level system: the ground $^2T_2$ and the excited $^2E$. Therefore, the excitation of electrons in the $Ti^{3+}$ ions by the $\lambda_{exc}$ = 400 nm (violet arrow) leads to the population of the $^2E$ excited level. Subsequently, after the nonradiative relaxation process to the bottom of the $^2E$ parabola, the radiative depopulation of the $^2E$ level to the $^2T_2$ ground state is observed as the deep red emission (red arrow). The $Ti^{3+}$ luminescence was found to be strongly thermally quenched; therefore, the emission and excitation spectra of $SrTiO_3$ and $SrTiO_3$:$Ln^{3+}$ nanocrystals were studied at 10 K (Fig. 2b and c). It was found that upon $\lambda_{exc}$ = 400 nm excitation wavelength only a very weak emission signal of a broad emission band associated with the $^2E\rightarrow{}^2T_2$ electronic transition of $Ti^{3+}$ was recorded. However, when the $La^{3+}$ or $Lu^{3+}$ are introduced, the

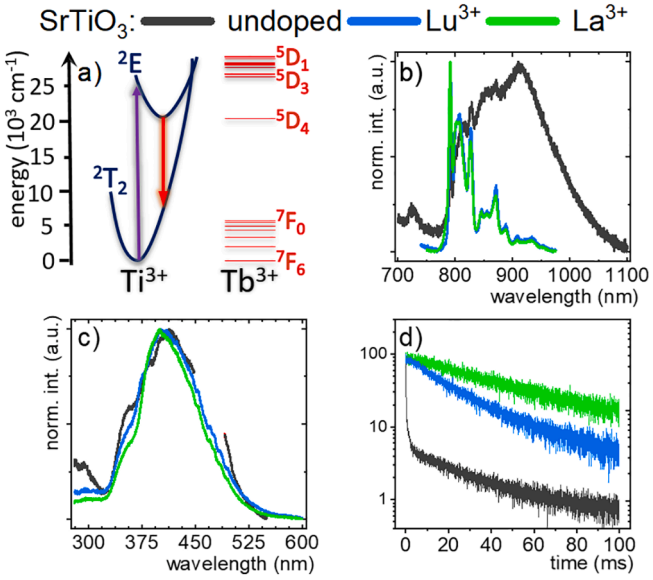


**Fig. 2.** Configurational coordinate diagram for $Ti^{3+}$ and $Tb^{3+}$ ions – a; the excitation spectra measured for $\lambda_{em}$ = 791 nm – b and the emission spectra excited by $\lambda_{exc}$ = 400 nm for $SrTiO_3$ undoped and doped with 0.1% $Lu^{3+}$ or 0.1% $La^{3+}$ ions measured at 10 K – c. Therefore the; the comparison of the luminescent decays of $^2E$ excited state of $Ti^{3+}$ ions for $SrTiO_3$ undoped and doped with $Lu^{3+}$ or $La^{3+}$ ions – d.

increase of the $Ti^{3+}$ emission intensity was observed with the change of the shape of the emission band. In the case of the $SrTiO_3$:$Lu^{3+}$ and $SrTiO_3$:$La^{3+}$ nanocrystals much narrower, with respect to the undoped counterpart, emission band centered at 800 nm with the clear vibronic structure was observed. It is difficult to quantitatively compare the emission intensities between the doped and undoped nanocrystals, but roughly an order of magnitude stronger signal was found for the $Ln^{3+}$ doped nanocrystals. A small number of $Ti^{3+}$ ions associated mainly with the surface states of the titanium ions and the distortion of their local ionic environment in the case of the $SrTiO_3$ nanocrystals results in their low emission intensity. However, the introduction of the $Ln^{3+}$ ions and, therefore, reduction of the $Ti^{4+}$ to $Ti^{3+}$, results in the increase of the $Ti^{3+}$ number and thus enhancement of $Ti^{3+}$ emission intensity observed for $SrTiO_3$:$Ln^{3+}$. Therefore in order to provide a qualitative comparison the normalized emission spectra are presented in Fig. 2b. The fact that the emission of the $Ti^{3+}$ was found even for the pure $SrTiO_3$ nanocrystals indicates that some traces of the $Ti^{3+}$ can be found in these crystals. Additionally, the broad emission band may suggest that it results from the superposition of the $Ti^{3+}$ ions localized in the different site symmetries, which can be found for example in the surface part of the nanocrystals. These findings agree with the previously reported studies on vanadium and titanium doped YAG nanocrystals and vanadium doped $LaGaO_3$ nanocrystals where different oxidation states of dopants were found at the surface part of the nanocrystals[36-38]. Also, it has been shown[39] that in the undoped $TiO_2$ nanocrystals Ti ions are trivalent ($Ti^{3+}$) at terminal planes of the crystal and tetravalent ($Ti^{4+}$) inside the crystal, as evidenced by the Electron energy loss spectroscopy. The results obtained in this work confirm that the presence of even the 0.1% $Ln^{3+}$ ions in the $Sr^{2+}$ site enables the stabilization of the octahedrally coordinated $Ti^{3+}$ ions. The comparison of low temperature excitation spectra of synthesized nanocrystals monitored at $^2E \rightarrow {}^2T_2$ transition ($\lambda_{em} = 791$ nm) for doped and undoped $SrTiO_3$ nanocrystals reveals a slight broadening of the $^2T_2 \rightarrow {}^2E$ absorption band for $SrTiO_3$ nanocrystals with respect to the doped ones. This effect results from the previously described ordering of the local symmetry surrounding the $Ti^{3+}$ ions induced by the presence of the $Ln^{3+}$ dopant (Fig. 2c, Figure S10, Figure S11). Additionally, a small spectral shift of the band's maximum was found from 411 nm (24 330 $cm^{-1}$) for $SrTiO_3$ to ~ 399 nm (25 060 $cm^{-1}$) for $SrTiO_3$:$La^{3+}$ nanocrystals. It should be noted here that the weak luminescence signal of $Ti^{3+}$ from the $SrTiO_3$ nanocrystals resulted in the occurrence of the scattering lines of the Xe lamp in the excitation spectrum. Therefore in order to eliminate this additional line from the spectrum the break was used (black curve in Fig. 2c). It was found that the inhomogeneously broadened excitation band is a superposition of two bands. This effect is especially clearly seen in the spectra measured at higher (77 K) temperature at which the emission intensity of $Ti^{3+}$ is partially quenched (Figure S12 Figure S13). The spectra consist of the band centered at 365 nm (27 310 $cm^{-1}$) and a band at 410 nm (24 354 $cm^{-1}$) which can be attributed to the $O^{2-} \rightarrow Ti^{4+}$ and $^2T_2 \rightarrow {}^2E$ absorption bands respectively. The decrease of the temperature results in the enhancement of the $^2T_2 \rightarrow {}^2E$ absorption intensity which overlaps and dominates over $O^{2-} \rightarrow Ti^{4+}$ one. Additionally, an increase of $La^{3+}$ and $Lu^{3+}$ ions causes the increase of the contribution of the $^2T_2 \rightarrow {}^2E$ band with respect to the $O^{2-} \rightarrow Ti^{4+}$ one in the excitation spectra, which results from the increase of the number of stabilized $Ti^{3+}$ ions in the $SrTiO_3$:$Ln^{3+}$ nanocrystals. To quantify observed changes their ratio was calculated as a function of the dopant concentration (Figure S10c):

$$\delta = \frac{\int I(\ ^2E \rightarrow\ ^2T_2(Ti^{3+}))d\lambda}{\int I(CT(Ti^{4+}))d\lambda} \quad (1)$$

When $Lu^{3+}$/$La^{3+}$ ions concentration increases, the values of the δ parameter increases up to 2.2 for 5% $Lu^{3+}$ and 2.62 for 5% $La^{3+}$ in respect to $\delta = 0.62$ for undoped $SrTiO_3$ nanocrystals. The increase of $Ln^{3+}$ ions does not cause any changes in the shape of the emission spectra of $SrTiO_3$:$Ln^{3+}$ nanocrystals (Figure S12 and Figure S13). The measurements of the luminescence decay profile of the $Ti^{3+}$ ions reveal that the obtained cure for $SrTiO_3$ nanocrystals is strongly non-exponential (Fig. 2d). However, the incorporation of $Ln^{3+}$ ions causes the change of the decay profile shape increasing its exponentiality for $SrTiO_3$:$Lu^{3+}$ and even more for $SrTiO_3$:$La^{3+}$. The average lifetime value calculated from the double exponential fitting shows that the elongation of $\tau_{avr}$ from $\tau_{avr} = 1.23$ for $SrTiO_3$ up to $\tau_{avr} = 41.59$ ms and $\tau_{avr} = 64.75$ ms was obtained when $Lu^{3+}$ and $La^{3+}$ dopant ions, respectively, were introduced to the nanocrystals.

The strong susceptibility of $Ti^{3+}$ luminescence in $SrTiO_3$:$Ln^{3+}$ nanocrystals to thermal quenching of emission intensity can be exploited in terms of luminescent thermometry. Therefore, the spectroscopic properties of the synthesized nanocrystals were investigated in a 77–350 K temperature range. The $^2E \rightarrow {}^2T_2$ emission band of $Ti^{3+}$ strongly decreases in intensity at elevated temperatures (Fig. 3a). The analysis of the thermal dependence of the integral emission intensity of $Ti^{3+}$ ions reveals that the initial increase in the temperature causes a slight increase in the emission intensity. However, at temperatures above 170 K quenching of the emission intensity occurs (Fig. 3b). On the other hand, in the case of the $SrTiO_3$:$La^{3+}$ the thermal quenching starts at 150 K, while for the $SrTiO_3$:$Lu^{3+}$ nanocrystals the initial increase in the emission intensity of the $Ti^{3+}$ luminescence was not found and its luminescence starts to be quenched above 100 K. In the case of the $Ti^{3+}$ ions, the thermal quenching of emission results from the thermally stimulated crossing of the intersection point between $^2E$ and $^2T_2$ parabolas followed by the nonradiative depopulation of the $^2E$ state. Since the value of the energy of this intersection point (so called activation energy) depends on the local ion environment (crystal field strength) even small changes in the local $Ti^{3+}$ symmetry may modify activation energy value and, thus, the emission thermal quenching rate. Hence, differences in the thermal quenching rates of $Ti^{3+}$ luminescence for $SrTiO_3$ and $SrTiO_3$:$Ln^{3+}$ nanocrystals may result from the doping-induced changes of the local structure around Ti. It is worth to emphasizing that for the $SrTiO_3$:$Ln^{3+}$ nanocrystals the $Ti^{3+}$ emission was completely quenched already at 275 K. To quantify the thermally induced changes in the integral emission intensities of the $Ti^{3+}$band, the relative sensitivity of the luminescent thermometer was calculated as follows:

$$S_R = \frac{1}{\Omega}\frac{\Delta\Omega}{\Delta T} \times 100\% \quad (2)$$

where ΔΩ represents the change in the Ω thermometric parameter corresponding to the ΔT change in temperature. In this case, the intensity I($Ti^{3+}$) was used as Ω (Fig. 3c, Figure S14, Figure S15). The maximal value of the $S_R$ in the case of the intensity based luminescent thermometer in $SrTiO_3$ nanocrystals was found around $S_R = 2.5\%\ K^{-1}$ at 250 K, while the spectacular enhancement of the thermometric properties was found for $SrTiO_3$:$La^{3+}$ and $SrTiO_3$:$Lu^{3+}$ for which $S_R = 3.5\%\ K^{-1}$ at 210 K and 4.6% $K^{-1}$ at 200 K were found, respectively. Additionally, for $SrTiO_3$:$Ln^{3+}$ emission intensity was much higher with respect to the undoped counterpart, also. To understand the role of the $Ln^{3+}$ ions in the thermal quenching process of the $Ti^{3+}$ emission intensity in $SrTiO_3$:$Ln^{3+}$ nanocrystals the analogous analysis has been performed for nanocrystals with different $Ln^{3+}$ concentrations (Figure S14 and S15). It is clearly demonstrated that the increase in $Ln^{3+}$ concentration results in the reduction in the temperature onset of $Ti^{3+}$ emission thermal quenching. In addition, when the concentration of $La^{3+}$ ions increases, the initial enhancement of the $Ti^{3+}$ emission intensity observed at elevated temperatures starts to be hampered, while for 5% of $La^{3+}$ ions this effect is not observed. The comparison of the excitation spectra measured at 77 K for different $Ln^{3+}$ concentration gives the insight into the this effect. In the case of the $SrTiO_3$:$Lu^{3+}$ the absorption band associated with the $^2E \rightarrow {}^2T_2$ absorption is slightly shifted toward shorter wavelengths. Therefore, the $\lambda_{exc} = 400$ nm excitation line matched almost perfectly with the maximum of this band, thus the enhancement in the intensity with the increase in temperature

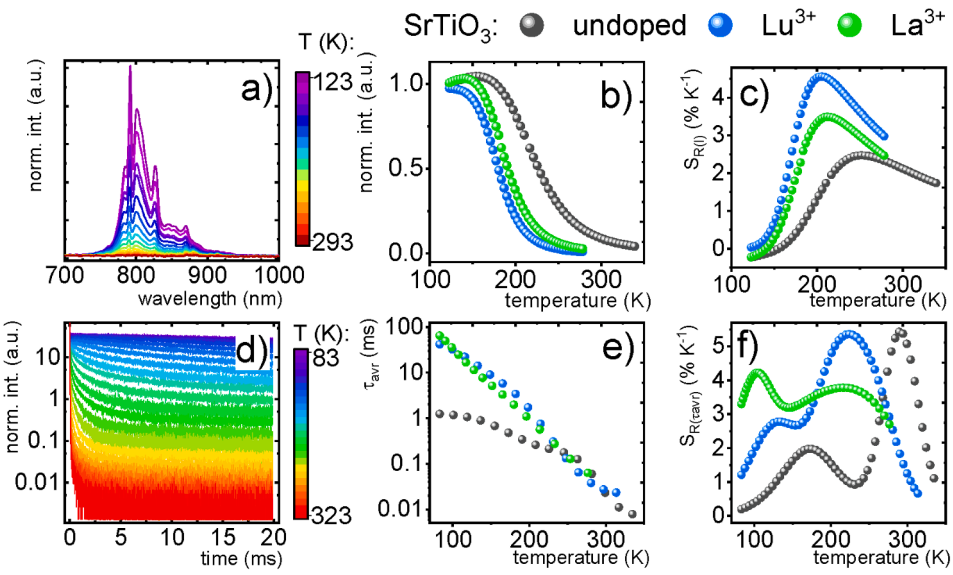


**Fig. 3.** Thermal evolution of the emission spectra for $SrTiO_3$:1% $Lu^{3+}$ sample – a; thermal evolution of the $Ti^{3+}$ band intensity – b and its sensitivity $S_{R(I)}$ for $SrTiO_3$ undoped and doped with 1% $Lu^{3+}$ or 1% $La^{3+}$ ions – c; thermal evolution of the luminescent decays of $^2E$ excited state of $Ti^{3+}$ ions for $SrTiO_3$:1% $Lu^{3+}$ sample – d; thermal evolution of the average decays $\tau_{avr}$ of $Ti^{3+}$ excited state – e and the relative sensitivity $S_{R(\tau avr)}$ for $SrTiO_3$ undoped and doped with 1% $Lu^{3+}$ or 1% $La^{3+}$ ions – f.

is not observed. However, when the same excitation wavelength matched the sideband of the absorption band of $Ti^{3+}$ ions in the $SrTiO_3$:$La^{3+}$ nanocrystals the electron–phonon coupling which leads to the broadening of the absorption band at elevated temperatures leads to the increase in the effective absorption cross section for the $\lambda_{exc} = 400$ nm excitation line. This effect is less evident when the intensity of the absorption band with respect to the charge transfer band of $Ti^{4+}$ increases as it was found for the higher $La^{3+}$ amount. The comparison of the $S_R$ calculated for different $Ln^{3+}$ concentration indicates that the 1% of $Lu^{3+}$ and 0.1% $Lu^{3+}$ ions are optimal dopant concentrations for thermometric application. It is worth noticing here, that although for the 5% of the $S_R$ were not the highest, the strong and constant thermal quenching rate of $Ti^{3+}$ luminescence in this case results in the relatively high $S_R > 1\%\ K^{-1}$ over the whole analyzed temperature range.

Since the emission intensity of a single band depends on many additional experimental factors, it exploitation for the remote temperature sensing is problematic. Nevertheless, the analysis of its thermal quenching rate is important from the understanding of the quenching mechanism process perspective. Nevertheless, to increase the reliability of remote temperature determination the kinetics of the $Ti^{3+}$ luminescence was analyzed as a function of temperature (Fig. 3d, Figure S16). Since the nonexponential decay profile was found, especially at high temperatures, the average lifetime calculated from the double exponential fit was used as a thermometric indicator in this case. It was found that in the case of the $SrTiO_3$ the $\tau_{avr}$ is gradually shortened at elevated temperatures; however, above 250 K much faster quenching rate can be observed. On the other hand, in the case of the $Ln^{3+}$ doped nanocrystals the strong shortening of the $\tau_{avr}$ is observed in the complete temperature range. The shortening of the $\tau_{avr}$ observed at low temperatures confirms that the enhancement of the $Ti^{3+}$ emission intensity at elevated temperatures observed in Fig. 3b results from the population mechanism described earlier in the text. Interestingly, when the $Lu^{3+}/La^{3+}$ content was increased, the slight elongation of the $\tau_{avr}$ is observed. For the $Lu^{3+}$ ions doped nanocrystals, the $\tau_{avr}$ changes from 29.0 to 41.1 ms for the range of 0.1–5% of $Lu^{3+}$ dopant, while $\tau_{avr}$ changes from 60.5 ms to 72.9 ms when the concentration of $La^{3+}$ increases from 0.1% $La^{3+}$ to 5% $La^{3+}$ (Fig. 3d, Figure S17, Figure S18). This effect can be explained in the decrease in the nonradiative decay rates of the $^2E$ state of $Ti^{3+}$ associated with the ordering of the local ions symmetry after the introduction of the $Ln^{3+}$ ions (Fig. 3e). Strong thermal shortening of the $\tau_{avr}$ is reflected in the high values of the $S_R$ calculated for the lifetime based luminescent thermometer (Fig. 3f). In this case the highest values of the SR was found to be $S_R = 5.50\%\ K^{-1}$ for $SrTiO_3$ at 290 K, $S_R = 5.42\%\ K^{-1}$ for $SrTiO_3$:$Lu^{3+}$ at 220 and $S_R = 4.2\%\ K^{-1}$ at 104 K for $SrTiO_3$:$La^{3+}$. It is worth mentioning that although the highest value of $S_R$ was found not for $SrTiO_3$:$La^{3+}$, in the case of these nanocrystals the $S_R > 2.7\%\ K^{-1}$ was found in the whole analyzed temperature range. Additionally, it should be emphasized that in the case of the thermal 2D imaging using the lifetime-based approach typically two images are captured with the exposure time shorter than the lifetime of the thermal probe. Therefore, the much shorter value of the $\tau_{avr}$ observed for $SrTiO_3$ limits the available acquisition time and thus the intensity of the signal. Therefore $SrTiO_3$:$Ln^{3+}$ nanocrystals reveal better performance for low temperature thermal imaging in the lifetime-based approach

To balance the limitation of both proposed approaches: the low reliability of temperature determination in the intensity-based approach and shorth acquisition time and, consequently, low intensity of the signal, the additional ratiometric approach has been proposed in which the luminescent signal of the optically active lanthanide ion co-dopant was used as an internal reference. The selection of $Ln^{3+}$ for as a reference single is purposeful and motivated by two aspects: (i) the emission intensity of $Ln^{3+}$ is much less susceptible to temperature changes with respect to the transition metal ions, (ii) $Ln^{3+}$ itself will facilitate the reduction of the $Ti^{4+}$ to $Ti^{3+}$ ions. The good candidate for being the internal luminescent reference should meet several requirements: (i) its emission intensity cannot be strongly quenched by the multiphonon processes at elevated temperatures, (ii) its emission bands cannot spectrally overlap with the $Ti^{3+}$ emission which may hamper the reliability of temperature readout, (ii) its excitation spectrum should enable the independent excitation of $Ln^{3+}$ and $Ti^{3+}$ ions. All these requirements are met by the $Tb^{3+}$ ions which configuration of energy levels diagram facilitates its excitation using $\lambda_{exc} = 400$ nm, the most intense band corresponding to the $^5D_4 \rightarrow {}^7F_5$ electronic transition is localized at 540 nm and the energy difference between metastable $^5D_4$ state and the next lower laying state (14 800 $cm^{-1}$) prevents luminescence thermal quenching in the temperature range considered in this study. Therefore, the $SrTiO_3$:$Tb^{3+}$ nanocrystals have been synthesized and analyzed (Fig. 4a). It is observed that the intensity of the $Ti^{3+}$ emission is quenched faster than emission intensity of $Tb^{3+}$ ions. The analysis of the thermal dependence of the $Ti^{3+}$ emission intensity for the $SrTiO_3$:$Tb^{3+}$ nanocrystals indicates that the intensity of $^2E \rightarrow {}^2T_2$ electronic transition is quenched faster with respect to the $La^{3+}$ and $Lu^{3+}$ counterparts which is probably associated with the interionic energy transfer between $Ti^{3+}$ and the $Tb^{3+}$ ions (Fig. 4b, Figure S19). Therefore, their luminescence intensity ratio can be used as a thermometric parameter:

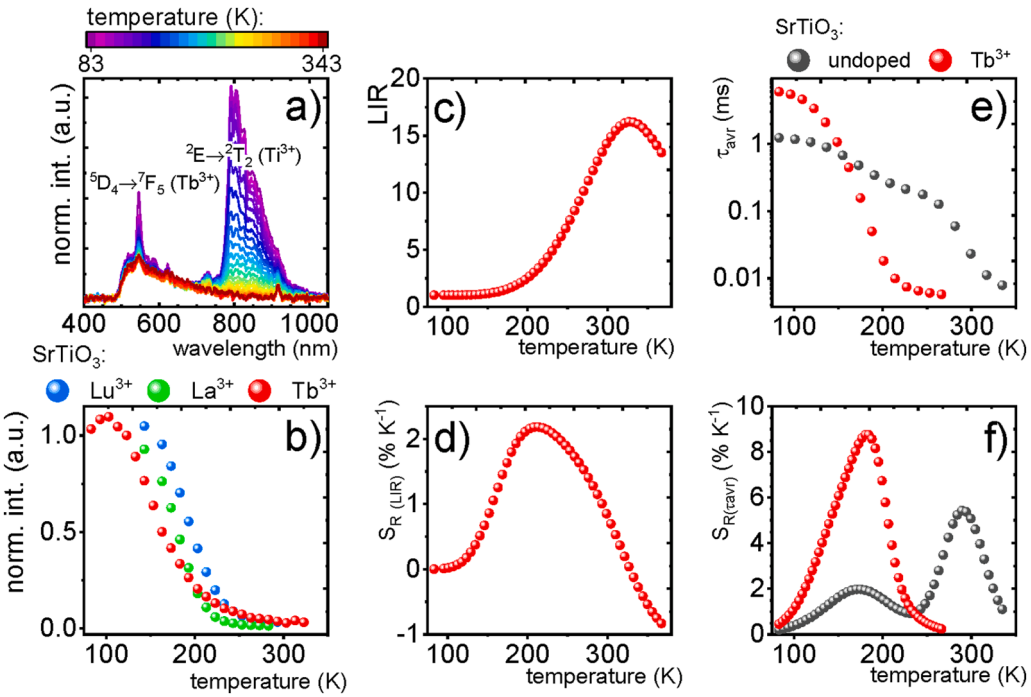


**Fig. 4.** Thermal evolution of the emission spectra for $SrTiO_3$:1% $Tb^{3+}$ sample – a; comparison of the thermal evolution of the $Ti^{3+}$ band intensity for different $Ln^{3+}$ dopants for $SrTiO_3$:$Ln^{3+}$ samples – b; thermal evolution of LIR – c and the relative sensitivity $S_R$(LIR) for $SrTiO_3$:1% $Tb^{3+}$ sample – d; comparison of the thermal evolution of average decays – e and its sensitivity $S_R(<\tau>)$ for $SrTiO_3$ undoped and doped with $Tb^{3+}$ ions – f.

$$LIR = \frac{\int I(Tb^{3+})d\lambda}{\int I(Ti^{3+})d\lambda} = \frac{\int I(\ ^5D_4 \rightarrow\ ^7F_5)d\lambda}{\int I(\ ^2E \rightarrow\ ^2T_2)d\lambda} \quad (3)$$

The 16-fold increase of the LIR was observed in the 77–330 K temperature range hence the maximal value of the $S_R = 2.20\%\ K^{-1}$ at 210 K was found in this case (Fig. 4c). The much lower $S_R$ obtained in the ratiometric approach with respect to the intensity-based counterpart results from the partial quenching of the $Tb^{3+}$ emission intensity (Fig. 4d). The $Ti^{3+} \rightarrow Tb^{3+}$ energy transfer can be exploited as an additional channel of the depopulation of the $^2E$ state of $Ti^{3+}$ which enables the improvement of the thermometric properties of the lifetime based luminescent thermometer. The much faster shortening of the $^2E$ state emission decay observed in the $SrTiO_3$:$Tb^{3+}$ nanocrystals (Fig. 4e) with respect to the $SrTiO_3$ counterpart results in the unprecedently high value of the $S_R = 8.83\%\ K^{-1}$ (at 180 K) for the lifetime based luminescent thermometers (Fig. 4f). The high repeatability of the obtained temperature readout verified within the several heating cooling cycles confirms the high thermometric performance of the $SrTiO_3$:$Ln^{3+}$ nanocrystals (Figure S20).

## 4. Conclusions

In this paper, the strategy of stabilization of $Ti^{3+}$ ions in the $SrTiO_3$ nanocrystals by the introduction of $Ln^{3+}$ ions was intensively explored. During the conducted research, it was found that in the nanocrystalline $SrTiO_3$ phosphors very weak and broad emission signal assigned to the luminescence of $Ti^{3+}$ ions is observed. The difference in the electric charge of the $Ln^{3+}$ ions substituting $Sr^{2+}$ site facilitates the reduction of the $Ti^{4+}$ to the $Ti^{3+}$ ions. Therefore, incorporation of the optically inactive $La^{3+}$ and $Lu^{3+}$ ions leads to the enhancement of the $Ti^{3+}$ emission intensity. The increase in the number of the $Ti^{3+}$ ions in the $SrTiO_3$ structure and the ordering of their local crystallographic environment was manifested also by the change of the shape of the $Ti^{3+}$ emission band and the elongation of the $^2E$ lifetime from $\tau_{avr} = 1.23$ for $SrTiO_3$ up to $\tau_{avr} = 64.75$ ms for $SrTiO_3$:$La^{3+}$ nanocrystals. Strong susceptibility of the $Ti^{3+}$ emission intensity to temperature changes was exploited in luminescent thermometry basing on the different approaches i.e. intensity of $^2E \rightarrow ^2T_2$ band, a lifetime of the $^2E$ state, and the luminescence intensity ratio of $Ti^{3+}$ and $Tb^{3+}$ ions. The maximal relative sensitivity of the luminescent thermometer based on the $Ti^{3+}$ emission intensity in $SrTiO_3$ nanocrystals was found to be $S_R = 2.5\%\ K^{-1}$ at 250 K. However, the introduction of $Ln^{3+}$ dopant enables the enhancement of the $S_R$ up to $4.6\%\ K^{-1}$ at 200 K for $SrTiO_3$:$Lu^{3+}$. In the case of the lifetime based luminescent thermometry the maximal value of the $S_R = 5.50\%\ K^{-1}$ was found for $SrTiO_3$ at 290 K, however, in the case of the $SrTiO_3$:$La^{3+}$ the $S_R > 2.7\%\ K^{-1}$ was found in the whole analyzed temperature range. Additionally, the strategy of ratiometric temperature readout using luminescence intensity ratio of $Ti^{3+}$ and $Tb^{3+}$ in $SrTiO_3$:$Tb^{3+}$ nanocrystals was evaluated. Although the relative sensitivity in this case was not very high, by the $Ti^{3+} \rightarrow Tb^{3+}$ energy transfer which additionally changes the population of the $^2E$ state of $Ti^{3+}$ ions leads to the improvement of the thermometric performance of the lifetime based luminescent thermometer. Hence the unprecedented $S_R = 8.83\%\ K^{-1}$ at 180 K was found for the $SrTiO_3$:$Tb^{3+}$ nanocrystals. All the results of conducted research clearly confirm the significant spectroscopic implication of coming from the $Ln^{3+}$ doping in $SrTiO_3$ nanocrystals and the high potential on the $Ti^{3+}$ based luminescent thermometer in $SrTiO_3$ nanocrystals for remote temperature sensing. However, further studies devoted to the enhancement of $Ti^{3+}$ emission intensity are desirable.

## Declaration of Competing Interest

The authors declare that they have no known competing financial interests or personal relationships that could have appeared to influence the work reported in this paper.

## Acknowledgements

The "High sensitive thermal imaging for biomedical and microelectronic application" project is carried out within the First Team program of the Foundation for Polish Science co-financed by the European Union under the European Regional Development Fund.

## Appendix A. Supplementary data

Supplementary data to this article can be found online at https://doi.org/10.1016/j.cej.2021.131165.

## References


[1] L. Marciniak, A. Bednarkiewicz, D. Kowalska, W. Strek, A new generation of highly sensitive luminescent thermometers operating in the optical window of biological tissues, J. Mater. Chem. C. 4 (24) (2016) 5559–5563.

[2] M. Back, J. Ueda, J. Xu, K. Asami, M.G. Brik, S. Tanabe, Effective ratiometric luminescent thermal sensor by $Cr^{3+}$-doped mullite $Bi_2Al_4O_9$ with robust and reliable performances, Adv. Opt. Mater. 8 (2020) 2000124.

[3] C. Wang, Y. Jin, L. Yuan, H. Wu, G. Ju, Z. Li, D. Liu, Y. Lv, L. Chen, Y. Hu, A spatial/temporal dual-mode optical thermometry platform based on synergetic luminescence of $Ti^{4+}$-$Eu^{3+}$ embedded flexible 3D micro-rod arrays: High-sensitive temperature sensing and multi-dimensional high-level secure anti-counterfeiting, Chem. Eng. J. 374 (2019) 992–1004.

[4] X. Chen, S. Liu, K. Huang, J. Nie, R. Kang, X. Tian, S. Zhang, Y. Li, J. Qiu, $Cr^{4+}$ activated NIR-NIR multi-mode luminescent nanothermometer for double biological windows, Chem. Eng. J. 396 (2020), 125201.

[5] M. Sekulić, Z. Ristić, B. Milićević, Ž. Antić, V. Đorđević, M.D. Dramićanin, $Li_{1.8}Na_{0.2}TiO_3$:$Mn^{4+}$: The highly sensitive probe for the low-temperature lifetime-based luminescence thermometry, Opt. Commun. 452 (2019) 342–346.

[6] W. Piotrowski, K. Trejgis, K. Maciejewska, K. Ledwa, B. Fond, L. Marciniak, Thermochromic luminescent nanomaterials based on $Mn^{4+}$/$Tb^{3+}$ codoping for temperature imaging with digital cameras, ACS Appl. Mater. Interfaces. 12 (39) (2020) 44039–44048.

[7] K. Maciejewska, L. Marciniak, Multimodal stokes and anti-stokes luminescent thermometers based on $GdP_5O_{14}$ co-doped with $Cr^{3+}$ and $Nd^{3+}$ ions, Chem. Eng. Journal. 402 (2020), 126197.

[8] M. Back, J. Ueda, H. Nambu, M. Fujita, A. Yamamoto, H. Yoshida, H. Tanaka, M. G. Brik, S. Tanabe, Boltzmann thermometry in $Cr^{3+}$ -doped $Ga_2O_3$ Polymorphs: The structure matters!, Adv. Opti. Mater. 9 (9) (2021) 2100033.

[9] D. Chen, Z. Wan, Y. Zhou, Dal-phase nano-glass-ceramics for optical thermometry, Sens. Actuators B. 226 (2016) 14–23.

[10] J.C. Chervin, B. Canny, M. Mancinelli, Ruby-spheres as pressure gauge for optically transparent high pressure cells, High Pressure Res. 21 (6) (2001) 305–314.

[11] Y. Fu, C. Li, F. Zhang, S. Huang, Z. Wu, Y. Wang, Z. Zhang, Site preference and the optical thermometry strategy by different temperature response from two sites environment of $Mn^{2+}$ in $K_7ZnSc_2B_{15}O_{30}$, Chem. Eng. J. 409 (2021), 128190.

[12] H. Luo, X. Li, X. Wang, M. Peng, Highly thermal-sensitive robust $LaTiSbO_6$:$Mn^{4+}$ with a single-band emission and its topological architecture for single/dual-mode optical thermometry, Chem. Eng. J. 384 (2020), 123272.

[13] M. Back, E. Trave, J. Ueda, S. Tanabe, Ratiometric optical thermometer based on dual near-infrared emission in $Cr^{3+}$-doped bismuth-based gallate host, Chem. Mater. 28 (22) (2016) 8347–8356.

[14] K. Elzbieciak-Piecka, J. Drabik, D. Jaque, L. Marciniak, $Cr^{3+}$ based nanocrystalline luminescent thermometers operating in a temporal domain, Phys. Chem. Chem. Phys. 22 (44) (2020) 25949–25962.

[15] K. Kniec, W. Piotrowski, K. Ledwa, M. Suta, L.D. Carlos, L. Marciniak, From quencher to potent activator – Multimodal luminescence thermometry with $Fe^{3+}$ in the oxides $MAl_4O_7$ (M = Ca, Sr, Ba), J. Mater. Chem. C. 9 (19) (2021) 6268–6276.

[16] G. Xiang, Q. Xia, X. Liu, Y. Wang, S. Jiang, L.i. Li, X. Zhou, L.i. Ma, X. Wang, J. Zhang, Upconversion nanoparticles modified by $Cu_2S$ for photothermal therapy along with real-time optical thermometry, Nanoscale. 13 (15) (2021) 7161–7168.

[17] G. Xiang, X. Liu, Q. Xia, S. Jiang, X. Zhou, L. Li, Y. Jin, L. Ma, X. Wang, J. Zhang, Deep-Tissue Temperature Sensing Realized in $BaY_2O_4$:$Yb^{3+}$/$Er^{3+}$ with Ultrahigh Sensitivity and Extremely Intense Red Upconversion Luminescence, Inorg. Chem. 59 (2020) 11054–11060.

[18] H. Suo, X. Zhao, Z. Zhang, C. Guo, Ultra-sensitive optical nano-thermometer $LaPO_4$: $Yb^{3+}$/$Nd^{3+}$ based on thermo-enhanced NIR-to-NIR emissions, Chem. Eng. J. 389 (2020), 124506.

[19] H. Suo, X. Zhao, Z. Zhang, Y. Wu, C. Guo, Upconverting $LuVO_4$:$Nd^{3+}$/$Yb^{3+}$/$Er^{3+}$@$SiO_2$@$Cu_2S$ Hollow Nanoplatforms for Self-monitored Photothermal Ablation, ACS Appl. Mater. Interfaces. 10 (2018) 39912–39920.

[20] V. Đorđević, M.G. Brik, A.M. Srivastava, M. Medić, P. Vulić, E. Glais, B. Viana, M. D. Dramićanin, Luminescence of $Mn^{4+}$ ions in $CaTiO_3$ and $MgTiO_3$ perovskites: Relationship of experimental spectroscopic data and crystal field calculations, Opt. Mater. 74 (2017) 46–51.

[21] D. Jaque, F. Vetrone, Luminescence nanothermometry, Nanoscale. 4 (15) (2012) 4301.

[22] A. Bednarkiewicz, L. Marciniak, L.D. Carlos, D. Jaque, Standardizing luminescence nanothermometry for biomedical applications, Nanoscale. 12 (27) (2020) 14405–14421.

[23] C.D.S. Brites, S. Balabhadra, L.D. Carlos, Lanthanide-based thermometers: At the cutting-edge of luminescence thermometry, Adv. Opt. Mater. 7 (2019) 1801239.

[24] C.D.S. Brites, P.P. Lima, N.J.O. Silva, A. Millán, V.S. Amaral, F. Palacio, L.D. Carlos, Thermometry at the nanoscale, Royal Soc. Chem. 4 (16) (2012) 4799.

[25] M.D. Dramićanin, Trends in luminescence thermometry, J. Appl. Phys. 128 (2020) 40902.

[26] M. Suta, A. Meijerink, A theoretical framework for ratiometric single ion luminescent thermometers—Thermodynamic and kinetic guidelines for optimized performance, Adv. Theor. Simul. 3 (2020) 2000176.

[27] K. Elzbieciak-Piecka, M. Suta, L. Marciniak, Structurally induced tuning of the relative sensitivity of $LaScO_3$:$Cr^{3+}$ luminescent thermometers by co-doping lanthanide ions, Chem. Eng. J. 421 (2021), 129757.

[28] M.P. Pechini, Method of preparing lead and alkaline earth titanates and niobates and coating method using the same to form a capacitor, 3330697, 1967.

[29] J. Liu, C.L. Wang, Y. Li, W.B. Su, Y.H. Zhu, J.C. Li, L.M. Mei, Influence of rare earth doping on thermoelectric properties of $SrTiO_3$ ceramics, J. Appl. Phys. 114 (2013), 223714.

[30] L. Tian, S. Il Mho, Enhanced luminescence of $SrTiO_3$:$Pr^{3+}$ by incorporation of $Li^+$ ion, Solid State Commun. 125 (2003) 647–651.

[31] L. Zhao, L. Fang, W. Dong, F. Zheng, M. Shen, T. Wu, Effect of charge compensation on the photoelectrochemical properties of Ho-doped $SrTiO_3$ films, Appl. Phys. Lett. 102 (2013), 121905.

[32] C. Jiang, L. Fang, M. Shen, F. Zheng, X. Wu, Effects of Eu substituting positions and concentrations on luminescent, dielectric, and magnetic properties of $SrTiO_3$ ceramics, Appl. Phys. Lett. 94 (2009), 071110.

[33] T. Kubo, H. Nozoye, Surface structure of $SrTiO_3$(1 0 0), Surf. Sci. 542 (3) (2003) 177–191.

[34] S. Okamoto, H. Kobayashi, H. Yamamoto, Enhancement of characteristic red emission from $SrTiO_3$:$Pr^{3+}$ by Al addition, J. Appl. Phys. 86 (1999) 5594.

[35] M.A. Peña, J.L.G. Fierro, Chemical structures and performance of perovskite oxides, Chem. Rev. 101 (7) (2001) 1981–2018.

[36] K. Kniec, L. Marciniak, The influence of grain size and vanadium concentration on the spectroscopic properties of YAG:$V^{3+}$, $^{V5}$+ and YAG: V, $L^{n3}$+ ($L^{n3}$+ = $E^{u3}$+, $D^{y3}$+, $N^{d3}$+) nanocrystalline luminescent thermometers, Sens. Actuators B. 264 (2018) 382–390.

[37] K. Kniec, L. Marciniak, Spectroscopic properties of $LaGaO_3$:V, $N^{d3}$+ nanocrystals as a potential luminescent thermometer, Phys. Chem. Chem. Phys. 20 (2018) 21598–21606.

[38] J. Drabik, B. Cichy, L. Marciniak, New type of nanocrystalline luminescent thermometers based on $Ti^{3+}$/$Ti^{4+}$ and $Ti^{4+}$/$Ln^{3+}$ ($Ln^{3+}$ = $Nd^{3+}$, $Eu^{3+}$, $Dy^{3+}$) luminescence intensity ratio, J. Phys. Chem. C. 122 (26) (2018) 14928–14936.

[39] B. Milićević, V. Đorđević, K. Vuković, G. Dražić, M.D. Dramićanin, Effects of $L^{i+}$ co-doping on properties of $Eu^{3+}$ activated $TiO_2$ anatase nanoparticles, Opt. Mater. 72 (2017) 316–322.